

**FORMATION OF STABLE GOLD
NANOPARTICLES VIA LASER ABLATION
CONJUGATED IN-SITU BY BSA IN HARSH
SALINE CONDITION FOR CELLS ANTI-
PROLIFERATIVE ACTIVITY**

SINAN ADNAN ABDULATEEF

UNIVERSITI SAINS MALAYSIA

2018

**FORMATION OF STABLE AuNPs VIA LASER
ABLATION CONJUGATED IN-SITU BY BSA IN
HARSH SALINE CONDITION FOR CELLS ANTI-
PROLIFERATIVE ACTIVITY**

by

SINAN ADNAN ABDULATEEF

**Thesis submitted in fulfillment of the requirements
for the degree of
Doctor of Philosophy**

March 2018

ACKNOWLEDGEMENT

In this memorable night in my life when I am going to finish the writing of this thesis, first I would like to express my thankfulness to Allah Almighty for granting me health with the capability to complete this research work. I would also like to dedicate this thesis to the soul of my father who sacrificed his soul for the homeland; God has mercy on him. Since 1982 until now, my mother has been supporting me. Without her, I am nothing. Along the way to the completion of this thesis, my wife, my daughters and my son all contributed in different ways. I am very thankful to all of them.

I would like to attribute special gratitude and appreciation to the persons below who made my research successful and who have assisted me at every point to achieve my goal:

My Supervisor, Dr. Ahmad Fairuz Omar with his vital support and assistance. His encouragement made it possible to achieve the goal.

Prof Mohd Zubir Mat Jafri. whose helped with his full effort at every point during my research to ensure my work is delivered in time.

Dr. Naser Mahmoud Ahmed with his cooperation, patience, and guidance during my study.

Dr. Azman Seenii, Research Director of Malaysian Institute of Pharmaceuticals and Nutraceuticals IPharm National Institute of Biotechnology Malaysia, whose reminders and constant motivation has encouraged me to meet the deadlines.

All the faculty staff in the engineering lab of the School of Physics and cell culture lab in Advanced Medical and Dental Institute USM, whose services have contributed to my research's success.

TABLE OF CONTENTS

ACKNOWLEDGEMENT	ii
TABLE OF CONTENTS	iii
LIST OF TABLES	viii
LIST OF FIGURES	ix
LIST OF ABBREVIATIONS	xiii
LIST OF SYMBOLS	xv
ABSTRAK	xvi
ABSTRACT	xviii
CHAPTER 1 - INTRODUCTION	
1.1 Introduction	1
1.2 The Problem Statement	4
1.3 Objectives of the Study	5
1.4 Hypothesizes of the Research	6
1.5 Thesis Outline	6
CHAPTER 2 - LITERATURE REVIEW: METALNPs AND THEIR	
2.1 Interactions between Lasers and Matter	8
2.1.1 Photothermal Mechanism	9
2.1.2 Photochemical Mechanism	10
2.2 Approaches to Synthesize the Nanomaterials	10
2.2.1 Bottom-Up Approach	11
2.2.2 Top-Down Approach	11

2.3	Pulse Laser Ablation (PLA)	13
2.4	Mechanisms of Pulse Laser Ablation in Liquid	14
2.5	Influence of Laser Parameters on the Outcome	19
2.5.1	Material Parameters	19
2.5.1(a)	Target Material	19
2.5.1(b)	Solvent	20
2.5.1(c)	Solutes	21
2.5.2	Laser Parameters	21
2.5.2(a)	Laser Wavelength	21
2.5.2(b)	Laser Fluence and Beam Spot Size	22
2.5.2(c)	Laser Pulse Duration	22
2.5.2(d)	Laser Irradiation Time	23
2.5.2(e)	Laser Repetition Rate	24
2.5.3	System Parameters	25
2.5.3(a)	Temperature	25
2.5.3(b)	System Pressure	25
2.6	Optical Properties of Metal Nanoparticles	26
2.6.1	Surface Plasma Resonance in Metal Nanoparticles	26
2.6.2	Dynamic Light Scattering (DLS)	28
2.7	AuNPs Aggregation, Surface Chemistry and Functionalization and Particle Stability	28
2.8	Human Blood Plasma and Simulated Body Fluid	32
2.9	Interactions of AuNPs with Bovine Serum Albumin	34
2.10	Interactions of AuNPs with Cells	34
2.10.1	Factors Influencing Cellular Effects of AuNPs	36

2.10.2	Dose- and Time-Dependent Effects	36
2.10.3	Size- and Shape-Dependent Effects	37
2.10.4	Surface Chemistry	38
2.11	Albumin-Conjugated Cytotoxic Drug NPs; Mechanism of Action in Cancer	39
2.11.1	The Albumin-Mediated GP60 Pathway	39
2.11.2	Protein AuNPs: Targeting the heart of the tumor	40
2.12	Apoptosis and Cell Cycle	41
2.12.1	Overview of programmed cell death	41
2.12.2	Overview of the Cell Cycle Process	43
CHAPTER 3 - METHODOLOGY AND INSTRUMENTATION		
3.1	Introduction	47
3.2	Preparation of Simulated Body Fluid	49
3.3	Preparation of AuNPs	52
3.4	Characterization Method	56
3.4.1	Spectroscopic Analysis (UV-Visible Spectroscopy)	56
3.4.2	Dynamic Light Scattering (DLS)	58
3.4.3	Fourier Transform Infrared Spectroscopy (FTIR)	62
3.4.4	High-Resolution Transmission Electron Microscopy (HR-TEM) and Selected area electron diffraction (SAED)	63
3.5	Cell Line	67
3.5.1	HeLa Cells	67
3.5.2	L929 Cells	67
3.5.3	Subculturing of Cells	68
3.5.4	Cryopreservation of Cells	68

3.5.5	Resuscitation of Frozen Cells	69
3.5.6	Cell Density Collection for Seeding	69
3.6	Microscopic Observation of Morphological Changes and Obtain of Cells Percent Confluence	70
3.7	Determination of Inhibitory Concentration (IC ₅₀)	71
3.7.1	Treatment of HeLa cells with Conjugated AuNPs with BSA in SBF	71
3.7.2	Trypan Blue Exclusion Assay	72
3.7.3	Cell Proliferation Assay	73
3.8	Cytotoxicity testing of AuNPs	74
3.9	Apoptosis Detection Assay by Flow Cytometry	75
3.10	Cell Cycle Analysis by Flow Cytometry	78
3.11	Statistical Analysis	80

CHAPTER 4 - RESULTS & DISCUSSIONS

4.1	Colloidal AuNPs Production	81
4.1.1	Absorption Spectra	81
4.1.2	High Resolution TEM Analysis	84
4.1.2(a)	AuNPs Prepared in SBF	85
4.1.2(b)	Ex-situ AuNPs Conjugated to BSA in SBF	86
4.1.2(c)	In-situ AuNPs Conjugated to BSA in SBF	89
4.1.2(d)	BSA Proteins Adsorb to AuNPs in SBF	91
4.1.3	Dynamic Light Scattering (DLS)	92
4.2	Stability of AuNPs	93
4.3	FTIR Spectra	95
4.4	Effective Laser Fluence to Synthesize AuNPs	97

4.4.1	Absorption Spectra	97
4.4.2	The Effect of Laser Fluence on AuNPs Morphology	102
4.4.3	Dynamic Light Scattering and Zeta Potential Measurement	106
4.5	Cytotoxicity Studies of the AuNPs Conjugated BSA in SBF on HeLa Cells	108
4.6	Antiproliferative Effect of AuNPs Conjugated with BSA in SBF	111
4.7	Cytotoxicity Test of AuNPs Conjugated with BSA in SBF at Laser Fluence 358.4J/cm ² on L929 Cells	113
4.8	Apoptotic Effects of AuNPs Conjugated with BSA in SBF on HeLa Cells	116
4.9	Effect of AuNPs Conjugated with BSA in SBF on Cell Cycle Phase of HeLa Cells	120
CHAPTER 5 - CONCLUSIONS AND FUTURE STUDIES		
5.1	Conclusions	122
5.2	Future Studies	124
REFERENCES		125
LIST OF PUBLICATION		

LIST OF TABLES

		Page
Table 2.1	High ionic composition of the human blood plasma and of SBF	33
Table 3.1	Composition of simulated body fluid	50
Table 4.1	Optical properties of AuNPs	100
Table 4.2	laser fluence, SPR, absorbance, AuNPs Weight and AuNPs concentration	101
Table 4.3	Dose-dependent cytotoxicity of the AuNPs conjugated BSA in SBF at laser fluence 358.4J/cm ² on HeLa cells	109
Table 4.4	Number of HeLa cell corresponded to untreated and growth suppression difference after treatment of the AuNPs conjugated BSA in SBF at laser fluence 358.4J/cm ² on HeLa cells	112
Table 4.5	Number of L929 cell corresponded to untreated and growth suppression difference after treatment of the AuNPs conjugated BSA in SBF at laser fluence 358.4J/cm ² on L929 cells	114
Table 4.6	Summary of induction of (cell percentage % distribution of Annexin V/PI staining) by AuNPs samples on HeLa cell, after 48h	119
Table 4.7	Cell cycle phase distribution (%) of untreated HeLa cells, AuNPs conjugated with BSA in SBF treated HeLa cells	120

LIST OF FIGURES

		Page
Figure 2.1	Bottom-up and the top-down approaches in synthesis of carbon-based nano materials	12
Figure 2.2	General mechanism of nanoparticle formation and growth during laser ablation synthesis in solution. Me, metal; L, liquid; * denotes excited and ionized states (reconstructed and modified from	18
Figure 2.3	Typical UV visible spectra of colloid dispersion containing of Ag nanoparticles, Au nanoparticles, and Cu nanoparticles obtained by PLA	27
Figure 2.4	Aggregation mechanism scheme. NaCl neutralizes the stabilizing electrostatic forces (EEs) on citrate-capped AuNPs, which in turn causes the van der Waals forces (Evdw) to drive the aggregate formation. When transferrin (k ₂) is added to the solution, it binds to the AuNP surfaces to shield them from the NaCl (k ₂), which prevents aggregation	31
Figure 2.5	Morphology change of programmed cell death process (Apoptosis and Necrosis)	46
Figure 3.1	Flowchart of research activity	48
Figure 3.2	Preparation of SBF	51
Figure 3.3	Schematic diagram of the PLAL system	53
Figure 3.4	Pure Au target (1g) 99.9% use to synthesize AuNPs by PLA	54
Figure 3.5	3 ml Colloidal AuNPs prepare inside vessel	54
Figure 3.6	Pulse laser ablation in Simulated Body Fluid system setup	55
Figure 3.7	UV-Visible spectrometer setup	57
Figure 3.8	Schematic of UV-Visible spectrometer	58
Figure 3.9	(a) DLS diagram (b) the electrical double layer and the zeta potential	61
Figure 3.10	FTIR spectrometer diagram	63

Figure 3.11	Schematic of a transmission electron microscope	65
Figure 3.12	Olympus Culture Microscopes Models CKX41 attached with camera serial (# 34114012)	70
Figure 3.13	(a) Cell counting kit-8 assay (CCK-8); (b) Apoptosis kit; (c) Schematically illustration of apoptosis detection assay	77
Figure 3.14	(a) Cell cycle kit; (b) Cell strainer mesh size is 35 μm	79
Figure 4.1	(a) UV-vis spectra of the colloidal dispersion containing particles synthesized by means of laser ablation of an Au target in situ (red line), and ex-situ (green line) at laser fluence 358.4J/cm ² . AuNPs + SBF is a (blue line) (b) in situ AuNPs+BSA+SBF (c) ex situ AuNPs+BSA+SBF (d) AuNPs+SBF	84
Figure 4.2	Transmission electron microscope images of AuNPs prepared in SBF with laser fluence 358.4 J/cm ²	86
Figure 4.3	HR-TEM of AuNPs conjugated with BSA in SBF using pulsed laser ablation technique. (a) The morphology (b) fringe spacing of 0.23 nm (c) selected area electron diffraction pattern indicating the face -center cubic (fcc) gold which is nanocrystalline in nature. In- situ at laser fluence 358.4 J/cm ²	88
Figure 4.4	HR-TEM of AuNPs conjugated with BSA in SBF using pulsed laser ablation technique. (a) The morphology (b) fringe spacing of 0.23 nm (c) selected area electron diffraction pattern indicating the face -center cubic (fcc) gold which is nanocrystalline in nature. In- situ at laser fluence 358.4 J/cm	90
Figure 4.5	BSA proteins adsorb to AuNPs synthesized by laser ablation in SBF In- situ at laser fluence 358.4 J/cm ²	91
Figure 4.6	Colloidal AuNPs distribution according to DLS for (a) ex-situ AuNCCs and (b) in-situ AuNPs conjugated to BSA in SBF at a laser fluence of 358.4 J/cm ²	93
Figure 4.7	UV-vis spectra measured over 4 weeks for the AuNPs conjugated BSA in SBF at laser fluence 358.4J/cm ² , demonstrating long-term stability	94
Figure 4.8	FTIR spectra of the free BSA in saline solution and adsorbed BSA (AuNPs-BSA system)	96
Figure 4.9	UV-vis spectra of a colloidal dispersion containing particles synthesized at different laser fluence	98

Figure 4.10	SPR intensity (black line) and AuNP concentration (red line) with laser fluence in AuNPs conjugated with BSA in SBF	99
Figure 4.11	UV-vis spectra of a colloidal dispersion containing particles synthesized by means of laser ablation of an Au target at 358.4 J/cm ² (focus), 238.8 J/cm ² (up from focus) and 259. J/cm ² (down from focus)	101
Figure 4.12	TEM images and size distributions of AuNPs conjugated with BSA prepared in SBF produced with laser fluences of (a) 27.5, (b) 82.7, (c) 192.9 and (d) 358.4 J/cm ²	103
Figure 4.13	TEM and size distribution of a colloidal dispersion containing particles synthesized by means of laser ablation of an Au target at (a) 259.5 J/cm ² (down from focus) and (b) 238.8 J/cm ² (up from focus)	105
Figure 4.14	Colloidal AuNP size (diameter) distribution according to DLS intensity at different fluences: (a) 27.5 (b) 82.7 (c)192.9 and (d) 358.4 J/cm ²	107
Figure 4.15	The IC45 values of the AuNPs conjugated BSA in SBF in HeLa cells	109
Figure 4.16	Cell morphology of HeLa cells with and without AuNPs conjugated BSA in SBF 358.4 J/cm ² on HeLa cells. Some morphological changes were (A) apoptotic bodies and (B) cell shrinkage. All pictures in 10X magnification	110
Figure 4.17	Growth inhibition of HeLa cells treated with AuNPs conjugated with BSA in SBF for 6 days of incubation periods. The values were represented in \pm SD of triplicates	112
Figure 4.18	Effect of AuNPs conjugated with BSA in SBF at laser fluence 358.4J/cm ² on L929 cells	114
Figure 4.19	Cell morphology of L292 with and without AuNPs sample treatment. All pictures in 20X magnification	115
Figure 4.20	Annexin V expression for AuNPs conjugated with BSA in SBF for 48 hours on HeLa cells. FITC-A (horizontal) and PI-A (vertical) showed Annexin V and PI stains intensity respectively. Q1: dead cells/debris, Q2: late apoptotic cells, Q3: live cells, Q4: early apoptotic cells.	118

- Figure 4.21 Cell distribution (%) based on Annexin V/PI staining. The percentage of apoptotic cells was determined by flow cytometry. Data are representative of three independent replicates, with similar results. The values represent means \pm SD of triplicate estimates. There was a significant difference between treated and untreated cells with respect to total apoptosis ($P < 0.05$) 119
- Figure 4.22 Effect of AuNPs conjugated with BSA in SBF on cell cycle phase of HeLa cells. The first peak represented G1 phase; the second peak represented G2M phase while the gap in between two peaks represented S phase 121

LIST OF ABBREVIATIONS

ATCC	American Type Cell Culture
ATM	Ataxia telangiectasia mutated protein
AuNCC	Gold Nanocrystalline clusters
AuNPs	Gold NPs
BSA	Bovine Serum Albumin
Caspase	Cysteine-aspartate Proteases
Cdc	Cell division cycle protein
CDK (Cdk)	cyclin-dependent kinase
Chk1	Checkpoint kinase 1
Chk2	Checkpoint kinase 2
CIN	Cervical intra neoplasia
DDS	Drug Delivery System
DLS	Light Dynamic Scattering
DMEM	Dulbecco's Modified Eagle Medium
DMSO	Dimethyl sulfoxide
DNA	Deoxyribonucleic acid
EGFR	Epidermal Growth Factor Receptor
FBS	Fetal Bovine Serum
FITC	Fluorescein isothiocyanate
FT-IR	Fourier-transform infrared spectroscopy
G0/G1	Resting phase/Gap1 phase
H-TEM	High-resolution Transmission Electron Microscope
IC ₅₀	concentration of an inhibitor where the response (or binding) is reduced by half

NP (NPs)	Nanoparticle (Nanoparticles)
PBS	Phosphate Buffered Saline
PCD	Programmed Cell Death
PLA	Pulsed Laser Ablation
PLAL	Pulsed Laser Ablation in Liquid
ROS	Reactive Oxygen species
S	Synthesize phase
SAED	Selected Area Electron Diffraction
SBF	Simulated Body Fluid
SCC	Squamous Cell Carcinoma
SD	Standard Deviation
SPR	Surface Plasmon Resonance
TBEA	Trypan blue exclusion assay
TBS	Tris Buffered saline

LIST OF SYMBOLS

Λ	wavelength
%	percentage
D	diameter
Nm	nanometer
$^{\circ}\text{C}$	degree Celsius
mL	milliliter
M	Molar: (number of moles per liter)
ρ	density
M.W	molecular weight
N	number of molecules
D_z	average particle size
S	scattering light intensity

PEMBENTUKAN AuNPs MELALUI ABLASI LASER BERKONJUGAT IN-SITU OLEH BSA DALAM KEADAAN SALIN KASAR UNTUK AKTIVITI ANTI-PROLIFERASI SEL

ABSTRAK

Koloid AuNP akan beragregat dan mendak dalam larutan garam di bawah kepekatan NaCl terhadap kebanyakan bendalir tubuh dan plasma darah. Penyelidikan ini memberi fokus kepada penyediaan nanopartikel emas (AuNP) berkoloid dengan kestabilan dan bioaktiviti tinggi dalam bendalir tubuh tersimulasi (SBF) yang hampir serupa dengan plasma darah yang bebas pencemaran melalui teknik kos rendah yang boleh dilakukan pada suhu bilik dalam tempoh masa yang singkat. Untuk mencapai tujuan ini, tiga objektif spesifik berikut telah dirancang: Pertama, untuk menghasilkan ampaiian berkoloid AuNP berkestabilan tinggi dalam media yang hampir sama dengan plasma darah dengan menggunakan teknik-teknik sintesis ablas laser berdenyut. Kedua, untuk menggunakan penghasilan in-situ sistem biokonjugat AuNP berkoloid - albumin serum bovin untuk ablas laser berdenyut. Untuk ini, albumin serum bovin dijerapkan ke permukaan AuNP untuk memperbaiki kestabilan dan mempertingkatkan bio-keserasiannya. Ketiga, untuk menilai aktiviti antikanser terhadap titisan sel kanser servikal manusia (HeLa). Laser denyat Q-Switch 6 nanosaat digunakan untuk menghasilkan ampaiian berkoloid AuNPs menerusi ablas laser. Pencirian sampel yang lengkap dan sistematik terhadap struktur, morfologinya (belauan elektron, mikroskop elektron transmudasi resolusi tinggi, sifat optik (penyerapan UV-Vis, penyerakan cahaya dinamik, dan spektroskopi inframerah jelmaan Fourier) serta sifat elektrik (keupayaan zeta) telah dijalankan. Pendekatan ablas laser membolehkan saiz, taburan saiz dan bentuk nanopartikel dikawal. Kesan pelbagai parameter laser terhadap

kecekapan ablasi seperti panjang gelombang laser, fluens laser dan bilangan denyutan laser dapat dikaji, ia berguna dalam kepekatan dan produktiviti. Dengan menggunakan panjang gelombang laser asas 1064 nm, satu kepekatan tinggi nanopartikel emas berkoloid bersaiz besar lebih kurang 10 nm, iaitu hampir dengan taburan saiz ketat 8nm, dihasilkan. Spektrum Resonan Plasmon Permukaan (SPR) menunjukkan satu puncak tunggal yang tajam sekitar 530 nm. Ini menyatakan penghasilan nanopartikel emas tulen berbentuk sfera dengan purata saiz 8 nm menerusi pengukuran UV-Vis biasa. Penambahan in-situ BSA ke dalam koloid sampel sebelum teknik ablasi laser menghasilkan AuNP yang lebih stabil dan taburan saiz yang sempit. Manakala penambahan ex-situ BSA pula menghasilkan kluster nanopartikel. Kesan antikanser AuNP berkonjugat dengan albumin serum bovin diletakkan di bawah aktiviti sitotoksik dengan menggunakan titisan sel HeLa. AuNP berkonjugat dengan albumin serum bovin menunjukkan kesan sitotoksik yang besar menentang sel-sel HeLa dengan nilai IC_{45} ($0.10 \mu\text{g. mL}^{-1}$) yang dikira serta ditentukan melalui kaedah TBEA. Cerakin perkembangbiakan sel selama 6 hari menunjukkan nanopartikel emas berkonjugat dengan albumin serum bovin adalah berkesan. Analisis sitometri aliran mengesahkan apoptosis teraruh dalam sel-sel HeLa.

**FORMATION OF STABLE AuNPs VIA LASER ABLATION CONJUGATED
IN-SITU BY BSA IN HARSH SALINE CONDITION FOR CELLS ANTI-
PROLIFERATIVE ACTIVITY**

ABSTRACT

Colloidal AuNPs is known to aggregate and precipitate in the saline solution below the NaCl concentration of many bodily fluids and blood plasma. This research focused on the preparation of high stability and bioactivity colloidal gold nanoparticles (AuNPs) in simulated body fluid (SBF), which can closely mimic the blood plasma that is free from contamination through a low-cost technique that can be done at room temperature within a short period of time. To achieve this aim, the following three specific objectives were designed; Firstly, to produce a high stability colloidal suspension of AuNPs in media close to blood plasma by using pulse laser ablation synthesis techniques. Secondly, to use in situ generation of the colloidal AuNPs - bovine serum albumin bioconjugated system for pulsed laser ablation. Here, bovine serum albumin is adsorbed to the AuNP surface to enhance the stability and to improve its biocompatibility. Thirdly, to evaluate the anti-cancer activity towards human cervical cancer cell lines (HeLa). Q – Switch laser pulse of 6 nanoseconds was employed to produce a colloidal suspension of AuNPs by laser ablation. Comprehensive, systematical characterization of the samples, for their structural, morphological (electron diffraction, high-resolution transmittance electron microscopy, optical properties (UV-Vis absorption, light dynamic scattering, and Fourier transform infrared spectroscopy) and electrical (zeta potential) properties, have been carried out. The laser ablation approach provides controllable process size, size distribution, and shape of NPs. Effects of laser fluence have been examined on the

ablation efficiency, which is useful in concentration and productivity. Using the fundamental laser wavelength of 1064 nm, a high concentration of colloidal AuNPs with a large size of about 10 nm, which is close to the narrow size distribution of 8 nm, was produced. The Surface Plasmon Resonant (SPR) spectra show a sharp and single peak around 530 nm, indicating the production of pure and spherical AuNPs with average size 8 nm by regular UV-vis measurements. The in-situ addition of BSA in the colloidal samples prior to laser ablation technique generate a more stable and narrow size distribution of AuNPs. While the ex-situ addition of the BSA has generated nanoparticles cluster. The anti-proliferative effect of the AuNP conjugated with bovine serum albumin was subjected to cytotoxic activity using HeLa cell lines. The AuNP conjugated with bovine serum albumin displayed significant cytotoxic effect against HeLa cells with the IC_{45} value ($0.10 \mu\text{g. mL}^{-1}$) calculated, was determined with TBEA method. The 6-day cell proliferation assay indicated the AuNP conjugated with bovine serum albumin is effective. Flow cytometry analysis confirmed induced apoptosis in HeLa cells.

CHAPTER 1

INTRODUCTION

1.1 Introduction

Nanotechnology is an interdisciplinary research field that combines physics, chemistry, biology, engineering and medicine that allows for the early detection, accurate diagnosis, and personalised treatment of cancer. In essence, nanotechnology is the fabrication, design and application of materials at a nanoscale range (1–100 nm). Nanomedicine is the application of nanotechnology for the diagnosis, treatment, and prevention of diseases [1]. However, NPs were used by the ancient cultures of Egypt and Rome to produce works of art [2-4]. Much of today 's nanotechnology is focused on the systematic synthesis and characterization of new nanomaterials with enhanced applications and properties. The synthesis of NPs has attracted considerable interest over the last decade owing to their potential applications in medicine, environmental remediation, and energy. Nanoparticle (NP) drug carriers can be made from a variety of different materials that can be natural, including starches and lipids; synthetic, such as polymers; or inorganic, such as AuNPs have been made using substances including liposomes, Au nanoshells, carbon nanotubes, and polymeric NPs. A major advantage of NP is their high ratio of surface area to volume ratio. The outer surface can be modified and functionalised to increase their stability, biocompatibility, and biodegradation. They also have a highly controllable shape and size that are easy to design and prepare [1]. They are sensitive to external stimuli, and can be designed with a wide variety of architectures and material formats [4,5]. Furthermore, the increased surface-to-volume ratio of NPs allows various agents to be attached to further strengthen their unique properties. NPs are small enough to easily enter cells, which

can be beneficial for specific cell-targeting therapies. Au nanoparticles (AuNPs) are a well-established nanomaterial with an interesting scientific history. AuNPs can be more easily programmed with unique physicochemical properties, such as optical or catalytic parameters, compared to their bulk counterparts. AuNP colloidal solutions come in two colours: intense red and purple or blue. It is noteworthy that the colour of the solution is indicative of the size of the particles. The intense red colour indicates the presence of particles with a diameter of less than 100 nm, whereas a blue or purple solution indicates the presence of larger particles [6,7]. AuNPs can be used to exploit a special interaction between light and a metal; exposure to the correct wavelength of light can induce its electrons to oscillate at the same frequency through an effect called surface plasmon resonance (SPR) [8,9]. AuNPs can be used to identify biomarkers in the diagnosis of liver, lung, and breast cancer [10], and are a potential carrier for cellular drug delivery. Furthermore, AuNPs have been widely used in research focusing on protein–NP interactions. Therefore, the synthesis of gold and silver nanomaterials through an efficient, affordable, and environmentally friendly method is an important area of research in biomedical nanotechnology. In this context, the green chemistry approach for the synthesis of NPs is a more eco-friendly, and therefore preferable, approach.

AuNPs have a long and interesting scientific history [11]. AuNPs were first used over two thousand years ago for aesthetic and medical applications [12]. Their colouring properties in ceramics and ruby glass fabrication are still utilised in modern times. The scientific approach for studying NPs was introduced in the middle of the nineteenth century by Michael Faraday, who created a preparation of dispersed gold colloids in a solution [12]. Since then, the amount of research into NPs has increased exponentially. Currently, one of the primary focuses in nanoscience research is

metallic NPs [13,14]. AuNPs are highly stable and are widely employed in contemporary nanoscience research [13]. Therefore, many methods have been developed to prepare particles with a specific size and purity [2].

In this study, the biocompatible and inert AuNPs were chosen as a model system to test the effects of size *in vitro*. AuNPs have been widely used in cell imaging [3] targeted drug delivery [4], cancer diagnostics, and therapeutic applications. Furthermore, AuNPs are an appropriate candidate for our study since various sizes and shapes can be easily synthesised. Because gold is not an intrinsic element in biological systems, it can be easily characterised through various analytical chemistry techniques such as ultraviolet (UV)-absorption spectroscopy and dark-field microscopy. Hence, AuNPs are the most suitable candidate to test the effects of NPs in biomedical applications.

In this study, *in vitro* studies have shown that AuNPs conjugated with BSA in a simulated body fluid (SBF) synthesised by laser ablation with a high stability, narrow size distribution, and uniform shape resulted in high rates of cell death. Such structures were toxic to cells, activating apoptosis inducers and anti-proliferative agents. The exact mechanism of toxicity is still being investigated, though several possible mechanisms have been identified. These include cell membrane disruption, reactive oxygen species (ROS) production, and the penetration of NPs into cells leading to cell death. The induction of apoptosis has been revealed as a causative factor in NP-elicited DNA damage. The generation of intracellular ROS has been cited [15] as a major cause of toxicity by NPs, where it damages cellular components such as membranes, proteins, lipids, RNA, and DNA. If ROS production is low, cells exhibit resistance and survive, but higher ROS levels lead to cell death.

1.2 The Problem Statement

The only known cures for the cancer are surgery and/or chemotherapy, both of which pose a substantial risk. Currently, the majority of cancers are treated through chemical- or radiation-based therapies. There are some disadvantages to these conventional treatments; although cancer cells are targeted, healthy cells are also affected by such treatments. This can cause major side effects, leading to slow recovery along with the social or economic problems that usually arise.

The traditional physics-based method of NP synthesis requires expensive experimental equipment, and stabilizing agents are needed for chemistry-based methods, many of which are toxic and can contribute to environmental pollution [16,17]. When working with NPs, it is always crucial to quantify their post-synthesis morphology, size, uniformity, and dispersal before attempting experiments. However, the NPs may aggregate in cell culture media and under physiological conditions upon exposure to high ionic strength and proteins, leading to unexpected rapid clearance from the blood, as well as nontoxicity [18,19]. This is because AuNPs do not have the high colloidal stability required to prevent particle agglomeration in harsh environment. In a medical context, particularly when applying NPs in biological fluids, it is always crucial to prepare AuNPs in clean environment [20] and to ensure the synthesized NPs remain stable within harsh environment [21] since particles aggregation may potentially have an effect on the biodistribution of the material and lead to adverse effects [22]. For that reason, it is also vital to quantify the post-synthesis morphology, size, uniformity, and dispersal of NPs before attempting experiments on biological samples.

Thus, the viability of treatments using nanomaterials are increasing in popularity and could be described as alternative treatments in a clinical setting.

Knowing the properties of certain materials may lead to their development and enhancement as alternative treatments. Nanomaterials synthesized using metals such as gold [23].

1.3 Objectives of the Study

The aim of this study was to synthesise a high stability, narrow size distribution, and uniformly shaped AuNP conjugated with BSA using pulse laser ablation in SBF. The anti-cell proliferative activity of AuNPs may present a therapeutic advantage in the treatment of cancer. In spite of abundant evidence at the molecular level and extensive preclinical and clinical studies, its therapeutic effectiveness remains a challenge owing to its low activity. Therefore, this study is focused on synthesis AuNPs in SBF by using pulse laser ablation technique. The stability and the biocompatibility are improved by using BSA. The AuNPs colloid in SBF was employed as an anti-proliferation activity by using human cervical cancer cell line.

The objectives of this research are as follows:

1. To synthesise a BSA-conjugated AuNP system in SBF, which simulates physiological conditions.
2. To control the size and uniform shape of AuNPs for improving the stability.
3. To optimize the laser setup in improving the formation rate and distribution of AuNPs
4. To examine the anti-proliferative activity of the AuNPs conjugated with BSA in cancer cells.

1.4 Scope of Study

This research proposed laser ablation method to synthesize stable colloidal AuNPs that is biocompatible and can potentially be applied for medical application. The laser used in the experiments has a fundamental wavelength specifically at 1064 nm. To ensure the stability of the generated AuNPs, the samples were prepared in BSA, protein that is known to assist in the stability of the synthesized AuNPs [24]. In this research, we are taking a step ahead by adding (SBF) in our medium, with the intention to prepare a medium that is compatible with human blood plasma. It is also known that laser fluence showed no influence on the photo-degradation of BSA [25]. Putting all these into constant, the focus of this research was then located in controlling the size, shape and size distribution as well as optimizing and improving the formation rate of AuNPs through varying the laser parameters. Finalising this important finding, the synthesized AuNPs was then examined on their toxicity and cells anti-proliferative activity, which was conducted on HeLa Cancer cells.

1.5 Thesis Outline

The thesis contains five chapters, the preparation, and study of AuNPs combined with bovine serum albumin against cells anti-proliferative activity. The first chapter presents background information on the cancer therapy, AuNPs (as an alternative medicine), and the aim and the objectives of this research. A literature review about AuNPs and the uses of pulse laser ablation in liquid (PLAL) in simulated body fluid and bovine serum albumin, as well as their applications for cancer therapy, will be discussed in the second chapter. This chapter is categorized into seven main sections: i) PLA mechanism and perimeter, ii) optical properties of metal NPs, iii) Comparison human blood plasma with SBF, iv) Effect high ionic strength to AuNPs, v) Interactions of AuNPs with BSA, vi) Interactions of AuNPs with cell, vii)

Albumin-Conjugated Cytotoxic Drug NPs, viii) Apoptosis and Cell Cycle. Chapter three includes the description of basic theories, chemicals, principles, and instruments which used throughout of this research. Chapter four covers the obtained results followed by discussion about four main subjects: i) Synthesise AuNPs using PLAL ii) improve AuNPs stability in SBF ii) Characterization of AuNPs; ii) the toxicity efficacy of bovine serum albumin-combined with AuNPs on HeLa cancer cells. The last chapter will cover a summary of the obtained results, some concluding remarks, and perspectives for future research.

CHAPTER 2

LITERATURE REVIEW: METAL NANOPARTICLES AND THEIR PROPERTIES

This chapter includes the survey of literatures review of interactions between lasers and matter (photothermal mechanism and photochemical mechanism), the description of approaches to synthesize the nanomaterials, the optical properties of metal nanoparticles, the details of the AuNPs aggregation, surface chemistry and functionalization and particle stability, the comparative between human blood plasma and simulated body fluid based on high ionic, the interactions of AuNPs with bovine serum albumin, the interactions of AuNPs with cells, The main information of albumin-conjugated cytotoxic drug NPs, mechanism of action in cancer, and apoptosis pathway and cell cycle process.

2.1 Interactions between Lasers and Matter

The interactions of laser radiation with matter is the most important concept for understanding the synthesis of nanomaterials using laser beams. The use of pulsed laser synthesis (PLS) to manufacture new nanomaterials involves the selection of the appropriate laser processing parameters with respect to the photophysical properties of the material to which it is applied. In this section, basic concepts regarding the most common interactions between laser radiation and matter are presented.

When a pulse laser beam interacts with a material in a liquid medium, gaseous medium, or vacuum, the incident light will be absorbed or reflected. The absorbed energy from the laser beam reacts with the matter in the form of a chemical and/or thermal process.

Generally, two major mechanisms can result from this laser-matter interaction: photothermal or photochemical. For interactions between the matter and laser, the following factors should be taken into consideration:

- The physical state of the material, i.e. solid, liquid, or gas.
- The type of material, i.e. insulator, semiconductor, or conductor.
- Laser beam parameters: beam diameter, laser fluence, pulse width, and excitation wavelength.
- Impurities, defects, and crystal structure of the solid material in dual-interface experiments.

2.1.1 Photothermal Mechanism

The photothermal mechanism refers to the thermal activation processes induced by a pulsed laser inside a material, where a phase change occurs due to an increase in the enthalpy and temperature of the system. An excitation spectrum is produced by the absorbed photon energy in the area of the focused pulsed laser. These types of excitations are known as the thermal explosion, pyrolytic effect, or photothermal effect, and are usually described based on their relaxation times. In photothermal processes, the evaporation of materials occurs at a higher laser fluence, which in turn creates a heterogeneous nucleation of vapour bubbles leading to normal boiling. In this situation, the rapid homogeneous nucleation and expansion of vapour bubbles leads to phase explosion or explosive boiling, which carries off the solid or liquid material fragments [25,26]. Therefore, PLS can be used to induce major changes in the irradiated material, opening new reaction products and chemical reaction pathways, and generating novel material microstructures, surface morphologies, phases, nanostructures, and evaporation characteristics [27].

2.1.2 Photochemical Mechanism

The photochemical mechanism is used for non-thermal reactions induced by photons strong enough to break the bonds between atoms and molecules to generate electrons and ions. When non-thermal processes are the most dominant, the system is described as photolytic or photochemical. Laser irradiation generates broad excitation spectra in intermediary states, which induces the decomposition of chemical bonds between the molecules of the material. In nanosecond- and femtosecond-pulsed lasers, direct ionisation and the formation of dense electron-hole plasmas lead to direct bond-breaking, multi-photon ionisation, tunnel ionisation, and explosive disintegration of the lattice through electronic repulsion, also known as the Coulomb explosion [28-32].

When both thermal and non-thermal processes contribute directly to the overall processing rate of the PLA system, the mechanism is referred to as photophysical [29-30,33].

2.2 Approaches to Synthesize the Nanomaterials

There are two major approaches for nanomaterial synthesis: top-down or bottom-up. The structure and properties of the synthesised NPs can be controlled, depending on the experimental conditions employed. Different elements during the synthesis of NPs allow for the control of particle geometry, particle size, the degree of particle agglomeration, and the doping ratio. These parameters give the synthesised material new chemical and physical properties for different applications. A deep understanding of the required approach is critical for the manufacture of new structures with unique properties. Many techniques have been reported for both approaches, such as chemical vapour deposition, sol-gel, PLS, sputtering, and mechanical milling. In

this chapter, we will focus on techniques using pulsed lasers. The difference between each approach is described in Figure 2.1.

2.2.1 Bottom-Up Approach

Many nanomaterials are synthesised through the interaction of atoms and/or certain molecular species through a set of chemical reactions [34]. The precursor is typically a liquid or gas that is ionised, dissociated, sublimated, or evaporated and then condensed to form an amorphous or crystalline NP. This approach produces NPs with a homogeneous chemical composition, fewer defects, particles with a narrow size distribution, and less contamination.

2.2.2 Top-Down Approach

This approach begins with a large bulk quantity of the material to be synthesised, which is then broken into smaller and smaller fragments or particles when a source of energy is applied. The energy applied can be mechanical, chemical, or thermal; other forms of energy can also be used, such as laser irradiation. Using pulsed laser ablation (PLA) and pulsed laser deposition (PLD), the energy is absorbed by the material and transformed into chemical and/or thermal energy to break the intermolecular bonds within the bulk material

Top-Down Approach

Bottom-Up Approach

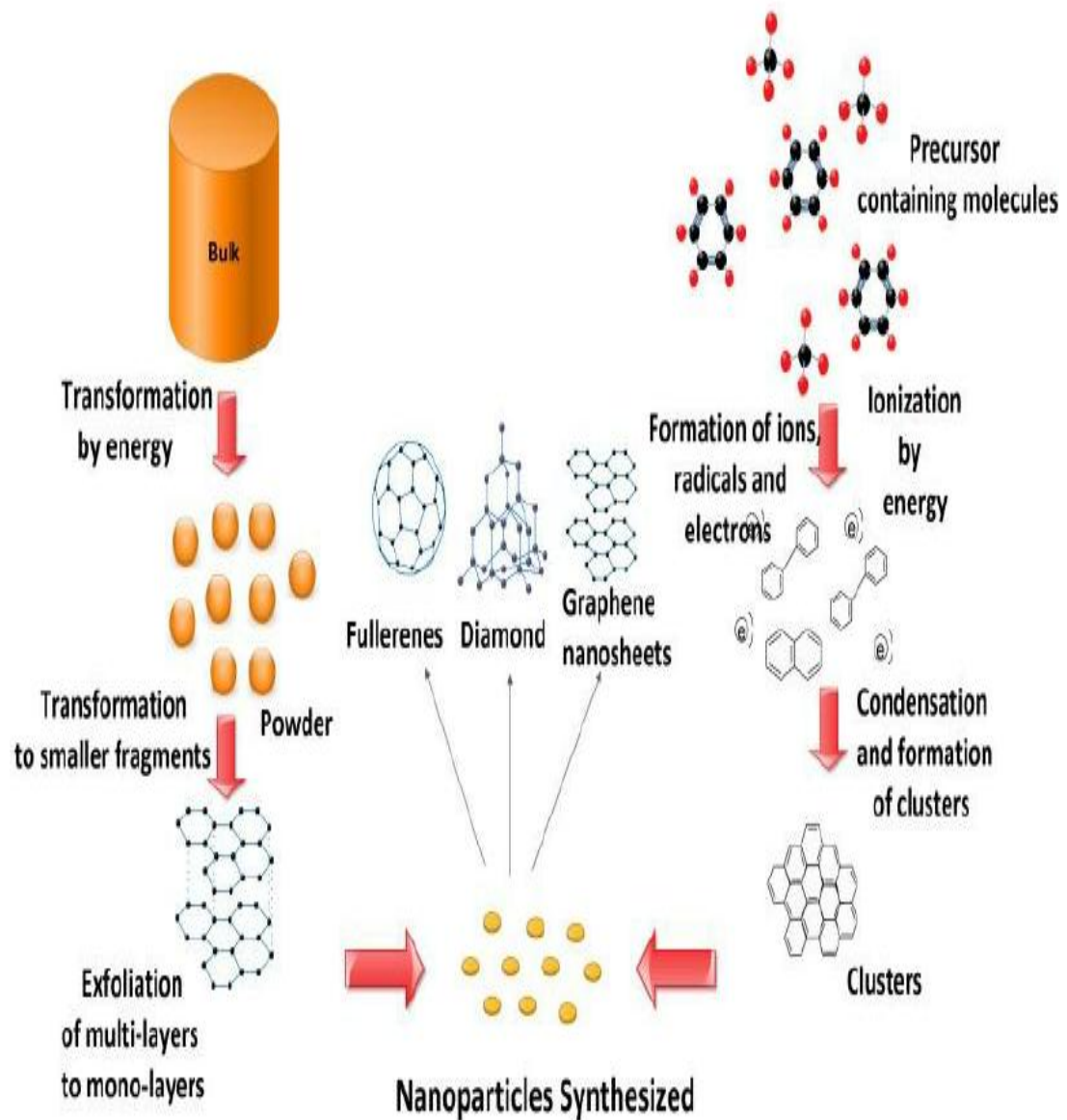


Figure 2.1: Bottom-up and the top-down approaches in synthesis of carbon-based nano materials [28].

2.3 Pulse Laser Ablation

Pulse Laser Ablation (PLA) is used for the top-down synthesis of nanomaterials such as nanotubes [34], nanowires [35], nanoribbons [36], quantum dots [37,38], and even nano-flakes of the material [38]. The technique is widely used by many researchers for the high-yield synthesis of both inorganic and carbon-based nanomaterials with varying particle sizes. PLA was first reported by Patil *et al.* in 1987 [38], who used PLA to form iron oxides with metastable phases from a pure iron target placed in water. Since then, many researchers have developed synthesis methods using liquid phase PLA (PLAL) and gas phase PLA (GP-PLA). A laser beam with a specific wavelength is focused by a lens through a transparent window of a reactor containing gas-solid or liquid-solid interfaces. When the laser beam hits the surface of the solid target (i.e. bulk or powder), the light interacts with the matter and generates a plume of NPs, which subsequently react with the gas or liquid. It is possible to dope the synthesised material by choosing a precursor containing the dopant element as a reactant during laser irradiation [39].

2.4 Mechanisms of Pulse Laser Ablation in Liquid

Although the processes involved in PLAL have been under investigation for several decades, the exact mechanism is still not well understood owing to the complexity of the technique in two primary stages: (1) the explosive ejection mechanism, in which a high-speed ejection of nanodroplets occurs and; and (2) the thermal evaporation mechanism, which is based on the formation of a plasma plume. Focusing the intense laser beam onto the bulk target material results in the delivery of a high-energy beam (absorption of photons) over a small region of the target material. This causes the ejection of solid fragments, highly excited species, and neutrals for

example, atoms, droplets, clusters, and ions (impact ionisation) from the surface, and a rapidly expanding plasma plume is formed. The amount of material removed from the target and the phase of the ejected material both depend on the absorbed energy E , as described by Momma *et al.* [40] To describe these processes, they use one-dimensional approximation and introduce the following notations: I , E are the absorbed laser intensity and energy, T , is the time dependent electron temperature, $\nu_{ei} \propto T_e^{-3/2}$ is the electron-ion collision frequency. they intentionally omit all constants in our formulas to make them more transparent. When the intense short-pulse laser radiation is focused onto the surface of a solid target, the plasma is produced on a very short time scale. Electrons are very rapidly heated by the short laser pulse, but ions remain cold, so that $T_e \gg T_i$. The growth of the electron temperature then can be found from the energy conservation law:

$$T_e \propto It/l \quad (t < \tau_l), \quad (2.1)$$

$$T_e \propto E/l \quad (t \geq \tau_l), \quad (2.2)$$

where l is the time dependent heat penetration depth inside the target. where l is the time dependent heat penetration depth inside the target. When $t > 1/\nu_{ei}$ the heat conduction into the target has a diffusion nature and is determined by the diffusion coefficient $D \propto v^2/\nu_{ei} \propto T_e^{5/2}$, where $v \propto T_e^{1/2}$ is the electron velocity. The heat penetration depth is in this case given by

$$l \propto (Dt)^{1/2} \propto T_e^{5/4} t^{1/2} \quad (2.3)$$

From equations ((1), (3) and (2), (3)) the following scaling laws can be derived

$$l \propto I^{5/9} t^{7/9}, T_e \propto I^{4/9} t^{1/2} \quad (t < \tau_l) \quad (2.4)$$

$$l \propto E^{5/9} t^{2/9}, T_e \propto E^{4/9} t^{-2/9} \quad (t \geq \tau_l) \quad (2.5)$$

As can be seen from (4) and (5), during the laser pulse the front of the electron thermal wave propagates faster (with the velocity $v_h \propto dl/dt \propto t^{-2/9}$) than after the laser pulse ($v_h \propto t^{-7/9}$).

The ablation depth per pulse is given by $L_a \propto v_a \tau_a \propto T_e^{1/2} \tau_a$. Using this relation and equation (5) with $t = \tau_a$ and $l = L_a$ we get a system of three “equations” for three unknown quantities. The solution of this system offers the following scaling laws

$$\tau_a \gg \tau_l, L_a \propto E^{2/3}, \tau_a \propto E^{1/2}, T_e \propto E^{1/3} \quad (2.6)$$

where L_a is the ablation depth, τ_a is the ablation duration, T_e is the electronic temperature during ablation, and τ_l is the laser pulse length.

The explosive ejection model was initially proposed to explain nanostructure formation of metal oxides and sulfides, in which the thermal evaporation model does not adequately describe their formation during PLAL, predominantly because millisecond pulsed lasers are used for synthesis. This deposits substantially lower power densities onto the target compared to nanosecond or femtosecond lasers. Explosive ejection occurs because the laser–target interaction causes the high-speed ejection of nanodroplets into the surrounding medium [41]. However, nanodroplet formation is not restricted to the use of millisecond lasers, but also depends on the target material. Nanodroplet formation was first observed by Tsuji *et al* [42], who irradiated Ag, Au, or Si targets in water with a nanosecond pulsed laser. They observed two distinct types of ejections at the target–water interface: (1) a straight jet emanating from the centre 100 μ s after the laser pulse, consisting of clusters and nanodroplets; and (2) a bubble confining the gas plasma that developed before 1 μ s and expanded until 200 μ s, which subsequently collapsed, leading to nucleation and particle growth. Phuoc *et al.* [43] proposed that the laser causes local melting, forming a molten drop,

and a high-pressure vapour or plasma is formed in the adjacent liquid. The explosive expansion of the vapour/plasma subsequently causes the molten drop to disintegrate into nanodroplets. These findings were confirmed by Yoo *et al.* [43], who observed that vapour formed near a superheated silicon mass during PLAL, which nucleated as bubbles. Upon reaching a critical size, rapid unlike the explosive ejection model, the thermal evaporation model proposes the formation of a plasma plume from the target plate material, because heating of the target material by the laser beam causes a phase transition in the target. A dense and highly energetic plasma plume that is at non-equilibrium is then formed. This plasma expands at a supersonic velocity and produces a shockwave that induces further increases in temperature and pressure within the plume and propagates through the target plate[44]. The plasma pressure and shockwave intensity depend on the laser wavelength, the thickness of the liquid layer, and the focusing conditions in water [45- 47]. In PLAL, the expansion of the plasma is confined by the liquid. This high-pressure plasma directly interacts with the target surface, causing additional ablation of the material (secondary ablation) during the first 100 ns; thereafter, the plasma pressure decreases [48]. After approximately 1 μ s, vaporisation of the liquid induces the formation of a cavitation bubble, which expands for 300 μ s and subsequently collapses, and releasing large amounts of energy at same time, which again causes ablation of the target (tertiary ablation) [48,49]. However, because the pressure after the collapse of the cavitation bubble is three to four orders of magnitude smaller than the pressure during the initial expansion of the plasma, the contribution of the tertiary ablation is substantially smaller than the primary and secondary ablation processes. In practice, thermal evaporation and explosive ejection are likely to occur at same time, or at least some features will overlap. Overall, NP formation follows a numberof steps based on nucleation and subsequent growth

mechanisms during plasma plume cooling. As shown in Figure Figure 2.2, the ablation process starts with an incoming pulse of laser light that deposits energy onto the target, which induces local heating and melting of the target material (1). This causes evaporation and ejection of the target material, which forms a plasma plume (2) that expands adiabatically (3). As the plasma plume starts to cool, supersaturation-driven nucleation occurs (4). Formation of the cavitation bubble is a result of the vaporisation of the liquid, which is in close contact with the hot plasma and spatially confines the plasma. The embryonic particle grows by attracting emitted materials such as atoms, clusters, and droplets (5) released from the target during PLAL (diffusion limited) as the cavitation bubble and plasma plume collapse (6) to yield the final product (7) [49-54].

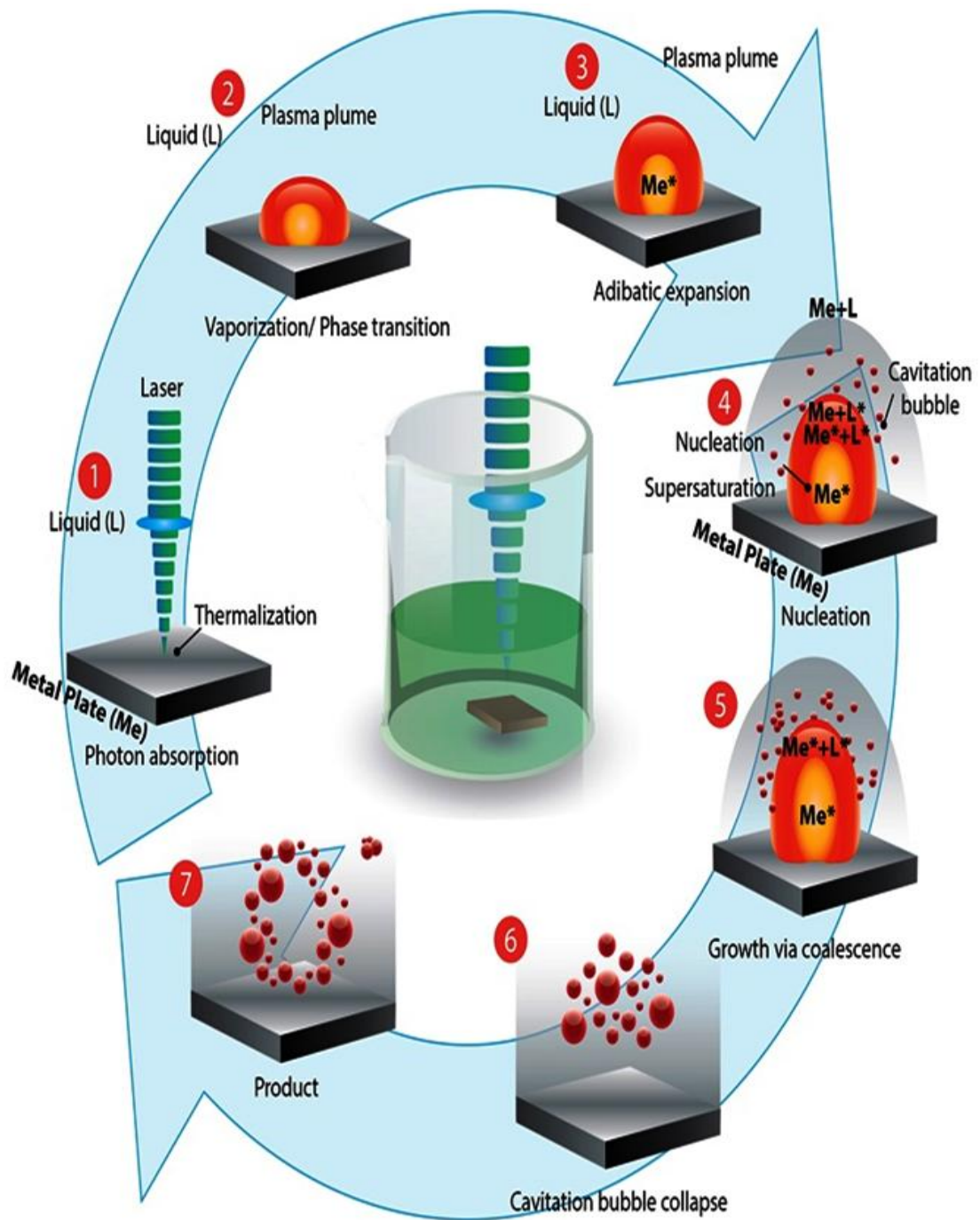


Figure 2.2: General mechanism of nanoparticle formation and growth during laser ablation synthesis in solution. Me, metal; L, liquid; * denotes excited and ionized states (reconstructed and modified from [55]).

2.5 Influence of Laser Parameters on the Outcome

PLAL is a versatile technique that allows high diversity in the synthesis of nanostructures without the need for chemicals that might negatively affect the properties (e.g., surface fouling, loss of eclectic stability) and toxicity profile of the product, even in trace amounts. Various environmental parameters directly affect nanostructure formation by influencing the initial ablation, nucleation, and/or particle growth, including laser parameters, the properties of the liquid environment, the presence of additives, and finally the bulk target itself. Overall, these parameters can be divided into two categories [55] : (1) material parameters and (2) laser parameters. Furthermore, PLAL strategies, such as repetitive irradiation (with the appropriate laser settings) of the colloidal solution, allowing cluster fragmentation (size distribution narrowing), reshaping, or further growth of the nanostructures, may cause the liquid environment to react with the nanostructure to produce surface-modified products. Alternatively, the presence of biocompatible additives may result in biocompatibilisation and/or biofunctionalisation of the product.

2.5.1 Material Parameters

The PLAL technique depends on the target material, solvent and solutes, which affect the size, shape, and size distribution of NPs.

2.5.1(a) Target Material

The bulk target material is a major parameter that determines many of the structural features of the produced nanostructure. Amendola and Meneghetti [51]. justifiably pointed out that, because of the complex sequential physicochemical phenomena involved in PLAL, the produced nanostructures do not necessarily have

the same phase and composition of the bulk target material. Furthermore, under the same experimental conditions, different materials have been reported to show distinctly different reactivities and yield different products. As stated previously, it should also be kept in mind that nanoscale properties can be quite different from the properties observed in the bulk material.

2.5.1(b) Solvent

The solvent strongly influences the composition of the produced nanostructures through confinement effects on the plasma plume, reactions with the nanostructure surface, and other physicochemical properties. PLAL of gold in pure water has been extensively investigated and yields relatively stable spherical colloids, which is a direct result of the presence of Au–O bonds on the surface [56,57] . However, these results also show that the conditions must have been oxidizing because of the reaction with oxygen from H₂O, or dissolved O₂ and CO₂. This example illustrates the impact of impurities on the solvent, which change the formation circumstances or induce reactions, especially with the nanostructure's surface. In organic solvents, such as tetrahydrofuran, ethanol, dimethyl sulfoxide, or acetonitrile, similar gold nanostructures are formed, albeit with lower average sizes and a higher propensity to agglomerate. The lower size might be a direct result of interference with nuclei coalescence due to the surrounding solvent (capping). Recently, a number of groups have shown that solvent degradation products absorb on the surface, such as polylys, enolates, and alcoholates, depending on the solvent used [58,60].

2.5.1(c) Solutes

Solutes (additives) generally change the physicochemical properties of the liquid solution, or physically and/or chemically interact with the ablated material. The addition of solutes to the liquid in which PLAL is performed has a direct impact on the cavitation bubble [61] and the confinement of the plasma plume [62]. The presence of the solute influences the viscosity, density, and surface tension of the solvent. This was clearly demonstrated by Yan *et al.* [61], who showed that nanoclusters from the target and bubbles from the liquid were formed during excimer PLAL, resulting in the formation of hollow nanospheres (the bubble interfaces trapped the nanoclusters). Recently, biological materials such as long-chain fatty acids (stearic, palmitic, and lauric acid), lauryl amine [63], chitosan [64], and starch [64] have been used as stabilisers in the synthesis of NPs. These stabilising agents prevent particle agglomeration by physically surrounding the NPs (capping), which results in charge and/or steric stabilisation.

2.5.2 Laser Parameters

The laser parameters are the most important parameters in PLA, and not only determines the ablation efficacy but also affords some control over the NP size.

2.5.2(a) Laser Wavelength

Laser wavelength is one of the most important parameters in PLAL, and not only determines the ablation efficacy, but also allows some control over the NP size. The relationship between the laser wavelength and particle size of metal NPs was extensively studied by Tsuji *et al.* [65]. They found that particle size and size distribution are directly proportional to the laser wavelength. Furthermore, the NP

formation efficiency increased with increasing wavelengths as a result of self-absorption and/or scattering by already formed NPs in the solution as PLAL progressed.

2.5.2(b) Laser Fluence and Beam Spot Size

The effect of laser fluence and beam size on the NPs produced during PLAL has been extensively studied, and numerous studies have shown that the laser fluence and beam size is directly proportional to the particle diameter and size distribution [40,66]. This effect occurs because both parameters directly affect the thermodynamic properties of the cavitation bubble and the produced plasma. An increase in these parameters not only increases the NP production rate and concentration at a near-linear rate, but also results in a considerably higher temperature and pressure in the plasma plume. Consequently, a longer cavitation bubble lifetime is obtained, and larger particles are formed.

2.5.2(c) Laser Pulse Duration

The pulse duration (τ_l) strongly influences NP structure, composition, and size distribution. Femtosecond lasers (10–15 fs) allow enhanced control over the particle size and offer high ablation efficiency. In contrast to picosecond (10–12 ps) and nanosecond (9–10 ns) lasers, substantially smaller particle sizes can be achieved with femtosecond lasers because the energy is transferred to electrons in the target over a time scale faster than electron–phonon thermalisation processes. Conversely, picosecond and nanosecond laser pulses transfer energy on a time scale comparable to that of thermal relaxation processes in the target. The plasma plume has a lifetime of 10–100 ns, [40,67]; thus, for nanosecond pulses, the plasma is present for nearly twice

the pulse duration [51]. The effect of pulse duration can be clearly observed when examining the craters formed at the target focal point. Femtosecond laser pulses form shallower craters with sharper borders compared to nanosecond laser pulses. This is indicative of ultra-fast localised heating and direct photoionisation processes. When the pulse length is 10 ps or more, the craters are less well defined, which points to the co-occurrence of direct photoionisation and thermal ablation processes (boiling, vaporisation, and rejection of melted material) [67]. As stated previously, with nanosecond pulses, the ablated material and the laser pulse coincide, resulting in an increase in plasma plume temperature, pressure, and lifetime. Under these conditions, melted drops ejected from the target plate into the plume are further vaporised. The craters formed by nanosecond laser pulses are deeper and have outer rims, which would be consistent with higher temperatures and increased formation efficiency.

2.5.2(d) Laser Irradiation Time

The laser irradiation time affects the size distribution of the NPs, since particle fragmentation as a result of a longer irradiation time decreases the average NP size, but increases the overall size distribution [68,69]. This effect was well illustrated by Takami *et al.* [70], who performed PLAL on AuNPs in an aqueous solution with a ns pulsed laser at 532 nm (210 mJ.cm^{-2} ; 10 min). The authors observed both a reduction in the particle size and a change in their shape: pre-irradiation, 19–47 nm; irregular and spheroid vs. post-irradiation, 5–21 nm; all spherical. These size reduction and shape-changing phenomena were likely due to heating from photon absorption via SPR on the particle surface. The energy was subsequently transferred to the lattice phonon, the temperature of the particle increased until the melting point was reached, and the particle melted to form a liquid droplet that eventually cooled to form a perfect

spherical NP with a reduced size. The size reduction itself was likely a result of surface vaporisation when the temperature exceeded the boiling point, causing atoms and small particles to be ejected.

2.5.2(e) Laser Repetition Rate

An important parameter that allows some control over the average NP size is the laser repetition rate, which defines the time interval (Δt_P) between consecutive laser pulses. The rate of NP formation per unit time increases at a near-linear rate as the repetition rate increases (this only applies when $\Delta t_P >$ cavitation bubble lifetime). For AuNPs, a linear relationship can be observed with repetition rates of 100–2,500 Hz (60 s laser ablation time) and a constant ablation efficiency [70]. At repetition rates reach the kHz range, the NP production rate deviates from linearity and the ablation efficiency decreases. This effect may be due to an increased local NP concentration, which results in the scattering of incoming laser pulses and negatively affects the ablation yield. Additionally, an increased local concentration and concomitant slow diffusion of the NPs promotes particle aggregation and coalescence. Overall, the laser repetition rate is an important parameter that can be used to steer the polydispersity of the colloidal solution and the final average particle size. However, a fundamental understanding of the impact of the laser repetition rate on NP formation, especially in terms of shielding, mass transport, focal residency time, and local temperatures, is still lacking explanations. especially when additives were used, contradictory results have been obtained.